Technical Design Report for the:
$\overline{\text{P}}$ANDA Data Acquisition and Event Filtring
(AntiProton Annihilations at Darmstadt)
Strong Interaction Studies with Antiprotons

$\overline{\text{P}}$ANDA Collaboration June 7, 2017

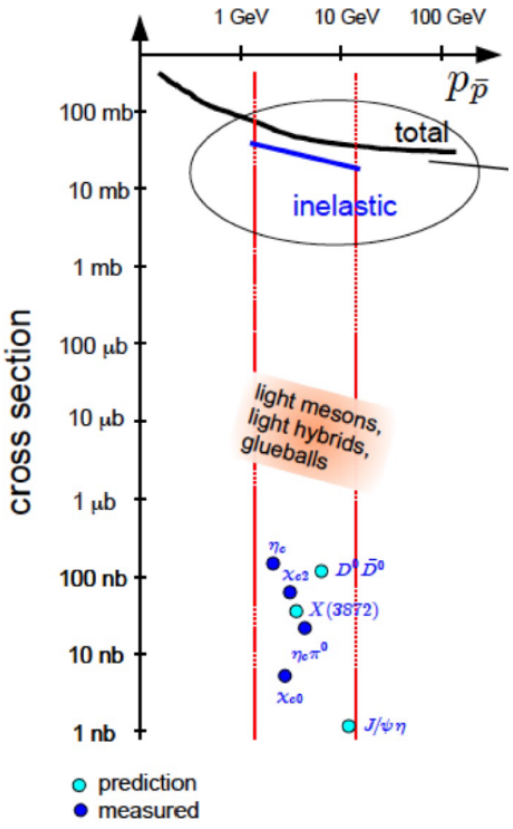

The $\overline{\text{P}}$ANDA Collaboration

2016-02-01 03:15:06

Aligarth Muslim University, Physics Department, **Aligarth**, India
B. Singh

Universität Basel, **Basel**, Switzerland
W. Erni, B. Krusche, M. Steinacher, N. Walford

Institute of High Energy Physics, Chinese Academy of Sciences, **Beijing**, China
H. Liu, Z. Liu, B. Liu, X. Shen, C. Wang, J. Zhao

Universität Bochum, Institut für Experimentalphysik I, **Bochum**, Germany
M. Albrecht, T. Erlen, M. Fink, F. Heinsius, T. Held, T. Holtmann, S. Jasper, I. Keshk, H. Koch, B. Kopf, M. Kuhlmann, M. Kümmel, S. Leiber, M. Mikirtychyants, P. Musiol, A. Mustafa, M. Pelizäus, J. Pychy, M. Richter, C. Schnier, T. Schröder, C. Sowa, M. Steinke, T. Triffterer, U. Wiedner

Rheinische Friedrich-Wilhelms-Universität Bonn, **Bonn**, Germany
M. Ball, R. Beck, C. Hammann, B. Ketzer, M. Kube, P. Mahlberg, M. Rossbach, C. Schmidt, R. Schmitz, U. Thoma, M. Urban, D. Walther, C. Wendel, A. Wilson

Università di Brescia, **Brescia**, Italy
A. Bianconi

Institutul National de C&D pentru Fizica si Inginerie Nucleara "Horia Hulubei", **Bukarest-Magurele**, Romania
M. Bragadireanu, M. Caprini, D. Pantea

P.D. Patel Institute of Applied Science, Department of Physical Sciences, **Changa**, India
B. Patel

University of Technology, Institute of Applied Informatics, **Cracow**, Poland
W. Czyzycki, M. Domagala, G. Filo, J. Jaworowski, M. Krawczyk, E. Lisowski, F. Lisowski, M. Michałek, P. Poznański, J. Płażek

IFJ, Institute of Nuclear Physics PAN, **Cracow**, Poland
K. Korcyl, A. Kozela, P. Kulessa, P. Lebiedowicz, K. Pysz, W. Schäfer, A. Szczurek

AGH, University of Science and Technology, **Cracow**, Poland
T. Fiutowski, M. Idzik, B. Mindur, D. Przyborowski, K. Swientek

Instytut Fizyki, Uniwersytet Jagiellonski, **Cracow**, Poland
J. Biernat, B. Kamys, S. Kistryn, G. Korcyl, W. Krzemien, A. Magiera, P. Moskal, A. Pyszniak, Z. Rudy, P. Salabura, J. Smyrski, P. Strzempek, A. Wronska

FAIR, Facility for Antiproton and Ion Research in Europe, **Darmstadt**, Germany
I. Augustin, R. Böhm, I. Lehmann, D. Nicmorus Marinescu, L. Schmitt, V. Varentsov

GSI Helmholtzzentrum für Schwerionenforschung GmbH, **Darmstadt**, Germany
M. Al-Turany, A. Belias, H. Deppe, R. Dzhygadlo, A. Ehret, H. Flemming, A. Gerhardt, K. Götzen, A. Gromliuk, L. Gruber, R. Karabowicz, R. Kliemt, M. Krebs, U. Kurilla, D. Lehmann, S. Löchner, J. Lühning, U. Lynen, H. Orth, M. Patsyuk, K. Peters, T. Saito, G. Schepers, C. J. Schmidt, C. Schwarz, J. Schwiening, A. Täschner, M. Traxler, C. Ugur, B. Voss, P. Wieczorek, A. Wilms, M. Zühlsdorf

Veksler-Baldin Laboratory of High Energies (VBLHE), Joint Institute for Nuclear Research, **Dubna**, Russia
V. Abazov, G. Alexeev, V. A. Arefiev, V. Astakhov, M. Yu. Barabanov, B. V. Batyunya, Y. Davydov, V. Kh. Dodokhov, A. Efremov, A. Fechtchenko, A. G. Fedunov, A. Galoyan, S. Grigoryan, E. K. Koshurnikov, Y. Yu. Lobanov, V. I. Lobanov, A. F. Makarov, L. V. Malinina, V. Malyshev, A.

G. Olshevskiy, E. Perevalova, A. A. Piskun, T. Pocheptsov, G. Pontecorvo, V. Rodionov, Y. Rogov, R. Salmin, A. Samartsev, M. G. Sapozhnikov, G. Shabratova, N. B. Skachkov, A. N. Skachkova, E. A. Strokovsky, M. Suleimanov, R. Teshev, V. Tokmenin, V. Uzhinsky, A. Vodopianov, S. A. Zaporozhets, N. I. Zhuravlev, A. G. Zorin

University of Edinburgh, **Edinburgh**, United Kingdom
D. Branford, D. Glazier, D. Watts

Friedrich Alexander Universität Erlangen-Nürnberg, **Erlangen**, Germany
M. Böhm, A. Britting, W. Eyrich, A. Lehmann, F. Uhlig

Northwestern University, **Evanston**, U.S.A.
S. Dobbs, K. Seth, A. Tomaradze, T. Xiao

Università di Ferrara and INFN Sezione di Ferrara, **Ferrara**, Italy
D. Bettoni, V. Carassiti, A. Cotta Ramusino, P. Dalpiaz, A. Drago, E. Fioravanti, I. Garzia, M. Savrie

Frankfurt Institute for Advanced Studies, **Frankfurt**, Germany
V. Akishina, I. Kisel, G. Kozlov, M. Pugach, M. Zyzak

INFN Laboratori Nazionali di Frascati, **Frascati**, Italy
P. Gianotti, C. Guaraldo, V. Lucherini

INFN Sezione di Genova, **Genova**, Italy
A. Bersani, G. Bracco, M. Macri, R. F. Parodi

Justus Liebig-Universität Gießen II. Physikalisches Institut, **Gießen**, Germany
K. Biguenko, K. Brinkmann, V. Di Pietro, S. Diehl, V. Dormenev, P. Drexler, M. Düren, E. Etzelmüller, M. Galuska, E. Gutz, C. Hahn, A. Hayrapetyan, M. Kesselkaul, W. Kühn, T. Kuske, J. S. Lange, Y. Liang, O. Merle, V. Metag, M. Nanova, S. Nazarenko, R. Novotny, T. Quagli, S. Reiter, J. Rieke, C. Rosenbaum, M. Schmidt, R. Schnell, H. Stenzel, U. Thöring, T. Ullrich, M. N. Wagner, T. Wasem, B. Wohlfahrt, H. Zaunick

University of Glasgow, **Glasgow**, United Kingdom
D. Ireland, G. Rosner, B. Seitz

Birla Institute of Technology and Science - Pilani , K.K. Birla Goa Campus, **Goa**, India
P.N. Deepak, A. Kulkarni

KVI-Center for Advanced Radiation Technology (CART), University of Groningen, **Groningen**, Netherlands
A. Apostolou, M. Babai, M. Kavatsyuk, P. J. Lemmens, M. Lindemulder, H. Loehner, J. Messchendorp, P. Schakel, H. Smit, M. Tiemens, J. C. van der Weele, R. Veenstra, S. Vejdani

Gauhati University, Physics Department, **Guwahati**, India
K. Dutta, K. Kalita

Indian Institute of Technology Indore, School of Science, **Indore**, India
A. Kumar, A. Roy

Fachhochschule Südwestfalen, **Iserlohn**, Germany
H. Sohlbach

Forschungszentrum Jülich, Institut für Kernphysik, **Jülich**, Germany
M. Bai, L. Bianchi, M. Büscher, L. Cao, A. Cebulla, R. Dosdall, A. Gillitzer, F. Goldenbaum, D. Grunwald, A. Herten, Q. Hu, G. Kemmerling, H. Kleines, A. Lehrach, R. Nellen, H. Ohm, S. Orfanitski, D. Prasuhn, E. Prencipe, J. Ritman, S. Schadmand, T. Sefzick, V. Serdyuk, G. Sterzenbach, T. Stockmanns, P. Wintz, P. Wüstner, H. Xu, A. Zambanini

Chinese Academy of Science, Institute of Modern Physics, **Lanzhou**, China
S. Li, Z. Li, Z. Sun, H. Xu

INFN Laboratori Nazionali di Legnaro, **Legnaro**, Italy
V. Rigato

Lunds Universitet, Department of Physics, **Lund**, Sweden
L. Isaksson

Johannes Gutenberg-Universität, Institut für Kernphysik, **Mainz**, Germany
P. Achenbach, O. Corell, A. Denig, M. Distler, M. Hoek, A. Karavdina, W. Lauth, Z. Liu, H. Merkel, U. Müller, J. Pochodzalla, S. Sanchez, S. Schlimme, C. Sfienti, M. Thiel

Helmholtz-Institut Mainz, **Mainz**, Germany
H. Ahmadi, S. Ahmed , S. Bleser, L. Capozza, M. Cardinali, A. Dbeyssi, M. Deiseroth, F. Feldbauer, M. Fritsch, B. Fröhlich, P. Jasinski, D. Kang, D. Khaneft, R. Klasen, H. H. Leithoff, D. Lin, F. Maas, S. Maldaner, M. Marta, M. Michel, M. C. Mora Espí, C. Morales Morales, C. Motzko, F. Nerling, O. Noll, S. Pflüger, A. Pitka, D. Rodríguez Piñeiro, A. Sanchez-Lorente, M. Steinen, R. Valente, T. Weber, M. Zambrana, I. Zimmermann

Research Institute for Nuclear Problems, Belarus State University, **Minsk**, Belarus
A. Fedorov, M. Korjik, O. Missevitch

Moscow Power Engineering Institute, **Moscow**, Russia
A. Boukharov, O. Malyshev, I. Marishev

Institute for Theoretical and Experimental Physics, **Moscow**, Russia
P. Balanutsa, V. Balanutsa, V. Chernetsky, A. Demekhin, A. Dolgolenko, P. Fedorets, A. Gerasimov, V. Goryachev

Nuclear Physics Division, Bhabha Atomic Research Centre, **Mumbai**, India
V. Chandratre, V. Datar, D. Dutta, V. Jha, H. Kumawat, A.K. Mohanty, A. Parmar, B. Roy, G. Sonika

Indian Institute of Technology Bombay, Department of Physics, **Mumbai**, India
S. Dash, M. Jadhav, S. Kumar, P. Sarin, R. Varma

Westfälische Wilhelms-Universität Münster, **Münster**, Germany
S. Grieser, A. Hergemöller, B. Hetz, A. Khoukaz, J. P. Wessels

Suranaree University of Technology, **Nakhon Ratchasima**, Thailand
K. Khosonthongkee, C. Kobdaj, A. Limphirat, P. Srisawad, Y. Yan

Budker Institute of Nuclear Physics, **Novosibirsk**, Russia
M. Barnyakov, A. Yu. Barnyakov, K. Beloborodov, A. E. Blinov, V. E. Blinov, V. S. Bobrovnikov, S. Kononov, E. A. Kravchenko, I. A. Kuyanov, K. Martin, A. P. Onuchin, S. Serednyakov, A. Sokolov, Y. Tikhonov

Institut de Physique Nucléaire, CNRS-IN2P3, Univ. Paris-Sud, Université Paris-Saclay, 91406, **Orsay cedex**, France
E. Atomssa, R. Kunne, D. Marchand, B. Ramstein, J. van de Wiele, Y. Wang

Dipartimento di Fisica, Università di Pavia, INFN Sezione di Pavia, **Pavia**, Italy
G. Boca, S. Costanza, P. Genova, P. Montagna, A. Rotondi

Institute for High Energy Physics, **Protvino**, Russia
V. Abramov, N. Belikov, S. Bukreeva, A. Davidenko, A. Derevschikov, Y. Goncharenko, V. Grishin, V. Kachanov, V. Kormilitsin, A. Levin, Y. Melnik, N. Minaev, V. Mochalov, D. Morozov, L. Nogach, S. Poslavskiy, A. Ryazantsev, S. Ryzhikov, P. Semenov, I. Shein, A. Uzunian, A. Vasiliev, A. Yakutin

IRFU,SPHN, CEA Saclay, **Saclay**, France
E. Tomasi-Gustafsson

Sikaha-Bhavana, Visva-Bharati, WB, **Santiniketan**, India
U. Roy

University of Sidney, School of Physics, **Sidney**, Australia
B. Yabsley

National Research Centre "Kurchatov Institute" B.P.KONSTANTINOV PETERSBURG NUCLEAR PHYSICS INSTITUTE, Gatchina, **St. Petersburg**, Russia
S. Belostotski, G. Gavrilov, A. Izotov, S. Manaenkov, O. Miklukho, D. Veretennikov, A. Zhdanov

Petersburg Nuclear Physics Institute of Russian Academy of Science, Gatchina, **St. Petersburg**, Russia
A. Kashchuk, O. Levitskaya, Y. Naryshkin, K. Suvorov

Stockholms Universitet, **Stockholm**, Sweden
K. Makonyi, M. Preston, P. Tegner, D. Wölbing

Kungliga Tekniska Högskolan, **Stockholm**, Sweden
T. Bäck, B. Cederwall

Sardar Vallabhbhai National Institute of Technology, Applied Physics Department, **Surat**, India
A. K. Rai

Veer Narmad South Gujarat University, Department of Physics, **Surat**, India
S. Godre

INFN Sezione di Torino, **Torino**, Italy
D. Calvo, S. Coli, P. De Remigis, A. Filippi, G. Giraudo, S. Lusso, G. Mazza, M. Mignone, A. Rivetti, R. Wheadon

Università di Torino and INFN Sezione di Torino, **Torino**, Italy
A. Amoroso, M. P. Bussa, L. Busso, F. De Mori, M. Destefanis, L. Fava, L. Ferrero, M. Greco, J. Hu, L. Lavezzi, M. Maggiora, G. Maniscalco, S. Marcello, S. Sosio, S. Spataro

Politecnico di Torino and INFN Sezione di Torino, **Torino**, Italy
F. Balestra, F. Iazzi, R. Introzzi, A. Lavagno, J. Olave

Università di Trieste and INFN Sezione di Trieste, **Trieste**, Italy
R. Birsa, F. Bradamante, A. Bressan, A. Martin

Uppsala Universitet, Institutionen för fysik och astronomi, **Uppsala**, Sweden
H. Calen, W. Ikegami Andersson, T. Johansson, A. Kupsc, P. Marciniewski, M. Papenbrock, J. Pettersson, K. Schönning, M. Wolke

The Svedberg Laboratory, **Uppsala**, Sweden
B. Galnander

Instituto de Física Corpuscular, Universidad de Valencia-CSIC, **Valencia**, Spain
J. Diaz

Sardar Patel University, Physics Department, **Vallabh Vidynagar**, India
V. Pothodi Chackara

National Centre for Nuclear Research, **Warsaw**, Poland
A. Chlopik, G. Kesik, D. Melnychuk, B. Slowinski, A. Trzcinski, M. Wojciechowski, S. Wronka, B. Zwieglinski

Österreichische Akademie der Wissenschaften, Stefan Meyer Institut für Subatomare Physik, **Wien**, Austria
P. Bühler, J. Marton, D. Steinschaden, K. Suzuki, E. Widmann, J. Zmeskal

---

Editors:	Wolfgang K"u hn	Email: w.kuehn@physik.uni-giessen.de
	Myroslav Kavatsyuk	Email: m.kavatsyuk@rug.nl
	N.N	
Technical Coordinator:	Lars Schmitt	Email: l.schmitt@gsi.de
Deputy:	Anastasios Belias	Email: a.belias@gsi.de
Spokesperson:	Klaus Peters	Email: klaus.peters@gsi.de
Deputy:	Tord Johansson	Email: tord.johansson@tsl.uu.se

Preface

This document describes the technical layout and the expected performance of the Data Acquisition system for the $\overline{\mathsf{P}}$ANDA experiment (Phase 1).

Contents

1 Executive Summary

The $\overline{\text{P}}$ANDA Experiment

$\overline{\text{P}}$ANDA [1] will be one of the four flagship experiments at the new international accelerator complex FAIR (Facility for Antiproton and Ion Research) in Darmstadt, Germany. With the $\overline{\text{P}}$ANDA detector unique experiments will be performed using the high-quality antiproton beam within a momentum range from 1.5 GeV/c to 15 GeV/c, stored in the HESR (High Energy Storage Ring) [2]. The exploration of fundamental questions of hadron physics in the charm and multi-strange hadron sectors will deliver essential contributions to many open questions of QCD. The scientific program of $\overline{\text{P}}$ANDA [3] includes hadron spectroscopy, properties of hadrons in matter, nucleon structure, hypernuclei and much more like the exotic bound quark states with or without gluonic degrees of freedom. The cooled antiproton beam colliding with a fixed proton or nuclear target will allow hadron production and formation experiments with a luminosity of up to $2 \times 10^{32}\,\text{cm}^{-2}\text{s}^{-1}$ in the fully completed version of the facility. In the Modular Start Version (MSV) the luminosity will be $1 \times 10^{31}\,\text{cm}^{-2}\text{s}^{-1}$. Excellent Particle Identification (PID) is mandatory for the success of the $\overline{\text{P}}$ANDA physics program, in which the Barrel TOF will play a crucial role.

$\overline{\text{P}}$ANDA Overview: Data Acquisition

The $\overline{\text{P}}$ANDA experiment adopts a free-running data acquisition concept in order to allow as much flexibility as possible which the complex and diverse physics objectives of the experiment require, and also to fully exploit the high interaction rate of up to 2×10^7 events/s. Each sub-detector system runs autonomously in a self-triggering mode, yet synchronised with a high-precision time distribution system, SODANET. Zero-suppressed and physically relevant signals are transmitted to a high-bandwidth computing network implementing a software trigger. Without a selection of data the whole data rate could be as high as 200 GB/s. The data acquisition system aims for an online data reduction of factor 100 – 1000.

Bibliography

[1] PANDA Collaboration. Technical Progress Report, FAIR-ESAC/Pbar. 2005.

[2] D. Prasuhn. Status HESR. PANDA meeting, June 2014.

[3] PANDA Collaboration. Physics Performance Report for PANDA: Strong Interaction Studies with Antiprotons. *arxiv:0903.3905*, 2009.

2 The $\overline{\text{P}}$ANDA Experiment

2.1 The $\overline{\text{P}}$ANDA Experiment

2.1.1 The Scientific Program

The $\overline{\text{P}}$ANDA (anti-Proton ANnihilation at DArmstadt) collaboration [1] envisages a physics core program [2] that comprises

- charmonium spectroscopy with precision measurements of mass, width, and decay branches;
- the investigation of states that are assumed to have more exotic configurations like multiquark states, charmed hybrids, and glueballs;
- the search for medium modifications of charmed hadrons in nuclear matter;
- the γ-ray spectroscopy of hypernuclei, in particular double Λ states.

In the charmonium and open-charm regions, many new states have been observed in the last years, that do not match the patterns predicted in those regimes [3]. There are even several states unambiguously being of exotic nature, raising the question about the underlying mechanism to form such kind of states [4].

The production of charmonium and open-charm states in e^+e^- interactions are restricted to initial spin-parities of $J^{PC} = 1^{--}$. This limits the possibility to precisely scan and investigate these resonances in formation reactions. The use of $\bar{p}p$ annihilation does not suffer from this limitation. Combined with the excellent energy resolution of down to about 25 keV, this kind of reactions offer unique opportunity to perform hadron and charmonium spectroscopy in the accessible energy range.

Since the decay of charm quarks predominantly proceeds via strangeness production, the identification of kaons in the final state is mandatory to separate the signal events from the huge pionic background.

2.1.2 High-Energy Storage Ring

The combination of HESR and $\overline{\text{P}}$ANDA are situated at FAIR facility (Fig. 2.1). The experiment aims at both high reaction rates and high resolution in order to be able to study rare production processes and small branching ratios. With a design value of 10^{11} stored antiprotons for beam momenta from 1.5 GeV/c to 15 GeV/c and high density internal targets the anticipated antiproton production rate of $2{\cdot}10^7\,\text{s}^{-1}$ governs the experiment interaction rate in the order of cycle-averaged $1{\cdot}10^7\,\text{s}^{-1}$. The stored antiprotons are freely coasting except for a 10% to 20% bunch structure allocated to a barrier bucket for compensation of energy losses.

Two complementary operating modes are planned, named *high luminosity* and *high resolution* mode, respectively. The high luminosity mode with $\Delta p/p = 10^{-4}$, stochastic cooling and a target thickness of $4 \cdot 10^{15}\,\text{cm}^{-2}$ will have an average luminosity of up to $L = 2 \cdot 10^{32}\,\text{cm}^{-2}\text{s}^{-1}$. For the high resolution mode $\Delta p/p = 5 \cdot 10^{-5}$ will be achieved with electron cooling for momenta up to $p = 8.9\,\text{GeV/c}$. Operation will mainly be in conjunction with a cluster jet target which will not impose a time structure onto the event rate. The cycle-averaged luminosity is expected to be $L = 2 \cdot 10^{31}\,\text{cm}^{-2}\text{s}^{-1}$.

2.1.3 Targets

The $\overline{\text{P}}$ANDA Target Spectrometer is designed to allow the installation of different targets. For hydrogen as target material both a Cluster-Jet target and a Pellet target are being prepared. One technical challenge is the distance of 2.1 m between the injection nozzle and the Interaction point, plus the same distance until the target particles are dumped in an efficient catcher keeping the whole target line under high vacuum.

The Cluster-Jet target is homogenous in space and time whereas a Pellet target with average inter-pellet spacing of 3 mm exhibits large density variations on the 10–100 μs timescale.

An extension of the targets to heavier gases such as deuterium, nitrogen, or argon is planned for complementary studies with nuclear targets.

2.1.4 Luminosity Considerations

The luminosity is directly linked to the number of stored antiprotons. The maximum luminosity depends on the antiproton production rate. The cycle-averaged antiproton production rate and reaction rate must be equal in the consumption limit. Due to injection losses and possible dumping of beam parti-

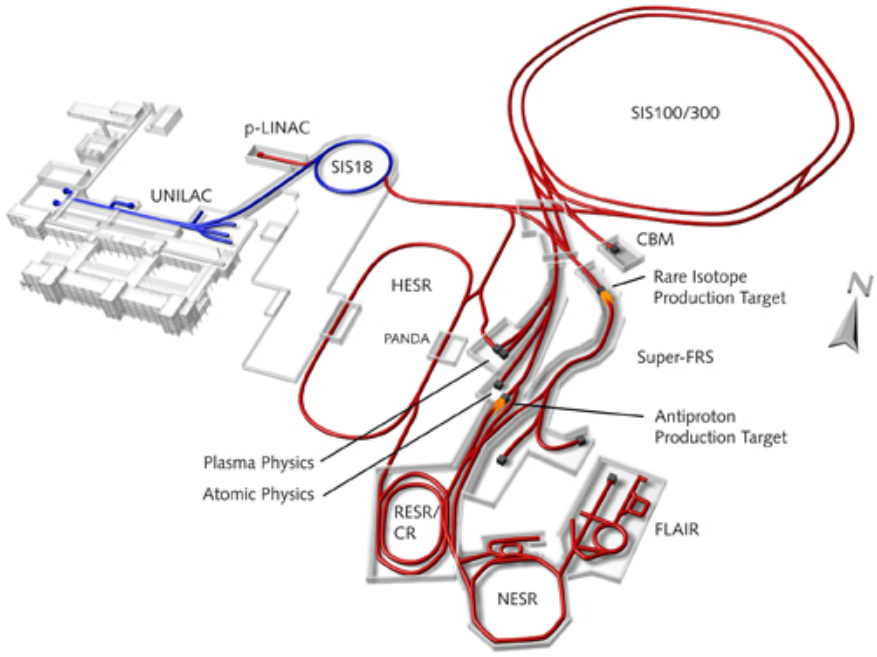

Figure 2.1: Schematic of the future FAIR layout incorporating the current GSI facilities on the left; on the right the future installations, the SIS 100 synchrotron the storage and cooler ring complex including CR and HESR and the Super FRS experiment being some of the new parts. $\overline{\text{P}}$ANDA is positioned right in the center of the image inside the HESR.

cles at the end of a cycle the time-averaged reaction rate will be lower. In Figure 2.2 the beam preparation periods with target off and data taking periods with target on are drawn. The red curve showing the luminosity at constant target thickness is proportional to the decreasing number of antiprotons during data taking. In order to provide a constant luminosity, compensation by adjusting the target thickness is studied.

In the case of a Pellet target, variations of the instantaneous luminosity will occur. These are depending on the antiproton beam profile, pellet size, pellet trajectories and the spacing between pellets. In the case of an uncontrolled pellet sequence target thickness fluctuations with up to 2–3 pellets in beam do occur during timescales of the pellet transit time which is 10–100 μs, . The pellet high luminosity mode (PHL mode) features smaller droplet size, lower spread in pellet relative velocity and smaller average pellet distance. The latter being much smaller than the beam size, hence the thickness fluctuations would be much reduced. However, this pellet target mode is currently being developed.

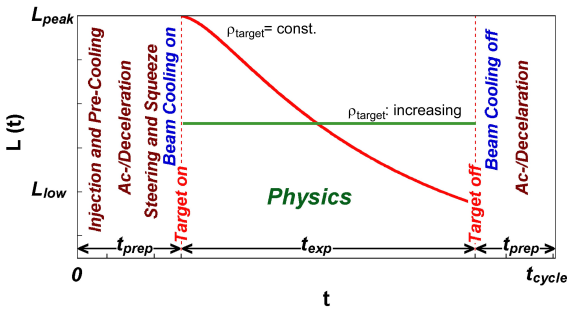

Figure 2.2: [5] Time dependent macroscopic luminosity profile $L(t)$ in one operation cycle for constant (solid red) and increasing (green dotted) target density ρ_{target}. Different measures for beam preparation are indicated. Pre-cooling is performed at 3.8 GeV/c. A maximum ramp of 25 mT/s is specified for acceleration and deceleration of the beam.

2.2 The $\overline{\text{P}}$ANDA Detector

Figure 2.3 shows the $\overline{\text{P}}$ANDA detector viewed with partial cut-outs. As a fixed target experiment, it is asymmetric having two parts, the Target Spectrometer (TS) and the Forward Spectrometer (FS). The antiproton beam is scattered off a pellet or cluster-

jet target (left side in Fig. 2.3). PANDA will measure $\bar{p}p$ reactions comprehensively and exclusively, which requires simultaneous measurements of leptons and photons as well as charged and neutral hadrons, with high multiplicities.

The physics requirements for the detectors are:

- to cover the full solid angle of the final state particles,
- to measure energy and momenta of the reaction products, and
- to identify particle types over the full range of momenta of the reaction products.

2.2.1 Target Spectrometer

Figure 2.4 shows a side view of the PANDA target spectrometer. The TS, which is almost hermetically sealed to avoid solid angle gaps and which provides little spare space inside, consists of a superconducting solenoid magnet with a field of 2 T and a set of detectors for the energy determination of neutral and charged particles as well as for the tracking and PID for charged tracks housed within the magnet. The silicon microvertex detector (MVD) closely abuts the beam pipe surrounding the target area and provides secondary vertex sensitivity for particles with decay lengths on the order of 100 μm.

The main tracker is a straw tube tracker (STT). There will be several gas electron multiplier (GEM) tracking stations in the forward direction. The tracking detectors like MVD and STT also provide information on the specific energy loss in their data stream.

Two Internally Reflected Cherenkov light (DIRC) detectors are to be located within the TS. Compared to other types of Ring Imaging Cherenkov (RICH) counters the possibility of using thin radiators and placing the readout elements outside the acceptance favors the use of DIRC designs as Cherenkov imaging detectors for PID. The Barrel DIRC covers the polar angles θ from 22° to 140° inside the PANDA TS. The Endcap Disc DIRC (EDD) covers the polar angles θ from 10° to 22° in the horizontal plane and 5° to 22°in the vertical plane. For the analysis of the DIRC data the tracking information is needed, as the Cherenkov angle is measured between the Cherenkov photon direction and the momentum vector of the radiating particle.

The Barrel TOF detector, which is the topic of this document, serves as precise (< 100 ps) timing detector cylindrically surrounding the target. It consists of small scintillator tiles read out by Silicon Photomultipliers (SiPMs) and is attached to the support frame outside of the Barrel DIRC providing reasonable π-K separation below 1 GeV/c (see chapter **??**).

The lead tungstate (PWO) crystals of the electromagnetic calorimeters (EMC) are read out with Avalanche Photo Diodes (APD) or vacuum pentodes. Both, the light output and the APD performance improve with lower temperature. Thus the plan is, to operate the EMC detectors at T = −25°C. The EMC is subdivided into backward endcap, barrel and forward endcap, all housed within the solenoid magnet return yoke.

Besides the detection of photons, the EMC is also the most powerful detector for the identification of electrons. The identification and measurement of this particle species will play an essential role for the physics program of PANDA.

The return yoke for the solenoid magnet in the PANDA TS is laminated to accommodate layers of drift tubes (Iarocci-type detectors) for the muon detection. They form a range stack, with the inner muon layer being able to detect low energy muons and the cumulated iron layer thickness in front of the outer layers providing enough hadronic material to stop the high energy pions produced in PANDA. A similar lamination and instrumentation of the iron is foreseen in the downstream door of the yoke augmented by the addition of a muon filter located in between the TS and the FS.

2.2.2 Forward Spectrometer

Figure 2.5 shows a side view of the PANDA forward spectrometer. The FS angular acceptance has an ellipsoidal form with a maximum angular acceptance of ±10 degrees horizontally and ±5 degrees vertically w.r.t. the beam direction.

The tracking section of the FS is incorporated into the large gap of a dipole magnet providing bending power of 2 Tm with a B-field perpendicular to the forward tracks. The other parts are placed further downstream outside the dipole magnet.

An aerogel RICH detector will be located right behind the dipole magnet followed by a the Forward Time-of-Flight wall (FTOF) which also covers the detection of slow particles below the Cherenkov light threshold. The energy is measured in the Shashlyk type electromagnetic calorimeter consisting of 1404 modules of 55 × 55 mm^2 cell size covering 2.97 × 1.43 m^2.

For the determination of the luminosity a detec-

tor based on four layers of monolithic active pixel sensors will be installed close to the beam pipe detecting scattered antiprotons under small angles.

2.2.3 The Particle Identification System

The charged particle identification (PID) will combine the information from the time-of-flight, tracking, dE/dx and calorimetry information with the output from the Cherenkov detectors, with their focus on positive identification of kaons.

The individual $\overline{\text{P}}$ANDA subsystems contributing to the PID and the combination of their data into a global PID information have been reviewed in the PID-TAG-report [6], a performance plot regarding the π-K separation power is shown in chapter **??**.

2.2.4 Data Acquisition

The data flow and processing is spatially separated into the Front End Electronics (FEE) part located on the actual detector subsystems and the Data Acquisition (DAQ), located off-detector in the counting room.

The FEE comprises analog electronics, digitization, low level pre-processing and optical data transmission to the DAQ system.

While each sub-detector implements detector specific FEE systems the DAQ features a common architecture and hardware for the complete $\overline{\text{P}}$ANDA detector.

Operating the PANDA detector at interaction rates of 2×10^7, typical event sizes of 4–20 kB lead to mean data rates of ~ 200 GB/second.

The PANDA DAQ [1] design does not use fixed hardware based triggers but features a continuously sampling system where the various subsystems are synchronized with a precision time stamp distribution system.

Event selection is based on real-time feature extraction, filtering and high level correlations.

The main elements of the PANDA DAQ are the data concentrators, the compute nodes and high speed interconnecting networks. The data concentrators aggregate data via point-to-point links from the FEE and the compute nodes provide feature extraction, event building and physics driven event selection.

A data rate reduction of about 1000 is envisaged in order to write event data of interest to permanent storage.

Peak rates above the mean data rate of ~ 200 GB/second and increased pile-up may occur due to antiproton beam time structure, target thickness fluctuations (in case of pellet target) and luminosity variations during the HESR operation cycle.

Therefore, FPGA based compute nodes serve as basic building blocks for the PANDA DAQ system exploiting parallel and pipelined processing to implement the various real-time tasks, while multiple high speed interconnects provide flexible scalability to meet the rate demands.

2.2.5 Infrastructure

The $\overline{\text{P}}$ANDA detector is located below ground in an experimental hall, encased in smaller tunnel-like concrete structure, partially fixed, partially made of removable blocks. Most subsystems connect their FEE-components via cables and tubes placed in movable cable ducts to the installations in the counting house, where three levels are foreseen to accommodate cooling, gas supplies, power supplies, electronics, and work space.

Bibliography

[1] PANDA Collaboration. Technical Progress Report, FAIR-ESAC/Pbar. 2005.

[2] PANDA Collaboration. Physics Performance Report for PANDA: Strong Interaction Studies with Antiprotons. *arxiv:0903.3905*, 2009.

[3] X. Liu. An overview of XYZ new particles. *arXiv:1312.7408v2 [hep-ph]*, 2014.

[4] Yu. S. Kalashnikova et al. Quark and Meson Degrees of Freedom in the $X(3872)$ Charmonium. *Phys. Atom. Nucl.*, 73, 2010.

[5] PANDA Collaboration. Straw Tube Tracker Technical Design Report. 2012.

[6] G. Schepers et al. Particle Identification at PANDA. *Report of the PID TAG*, March 2009.

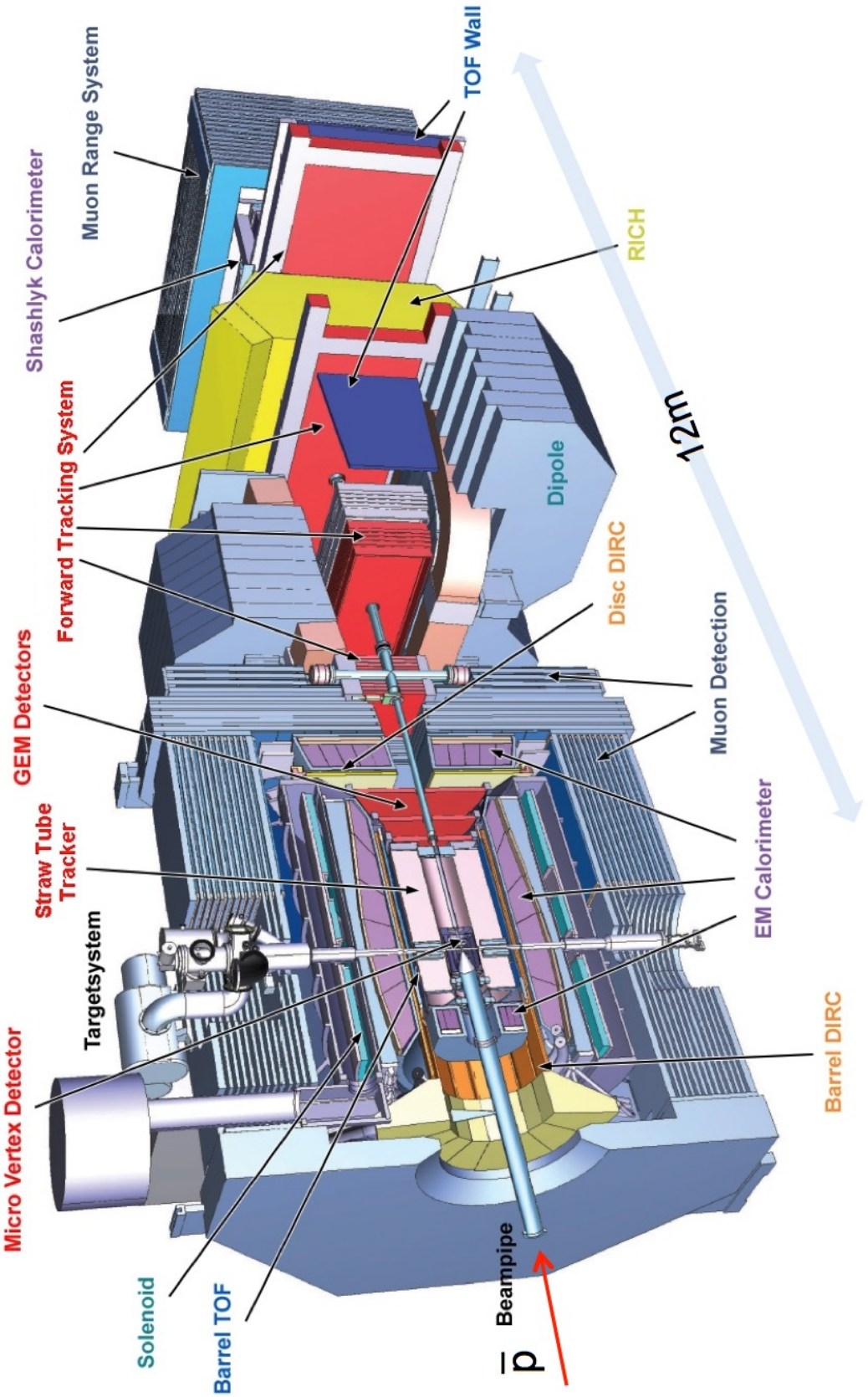

Figure 2.3: Aerial view of $\overline{\mathsf{P}}$ANDA with the Target Spectrometer (TS) on the left side, and the Forward Spectrometer (FS) starting with the dipole magnet on the right. The antiproton beam enters from the left.

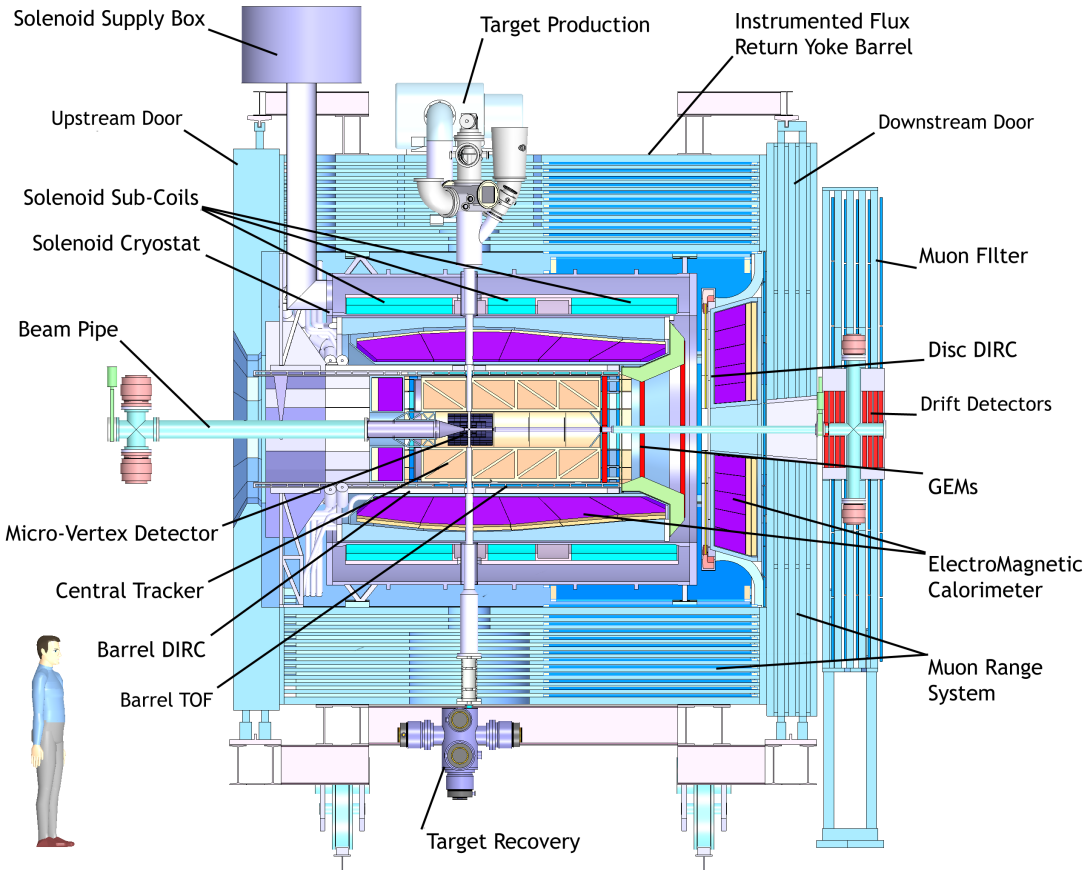

Figure 2.4: Side view of $\overline{\text{P}}$ANDA with the Target Spectrometer (TS). The antiproton beam enters from the left.

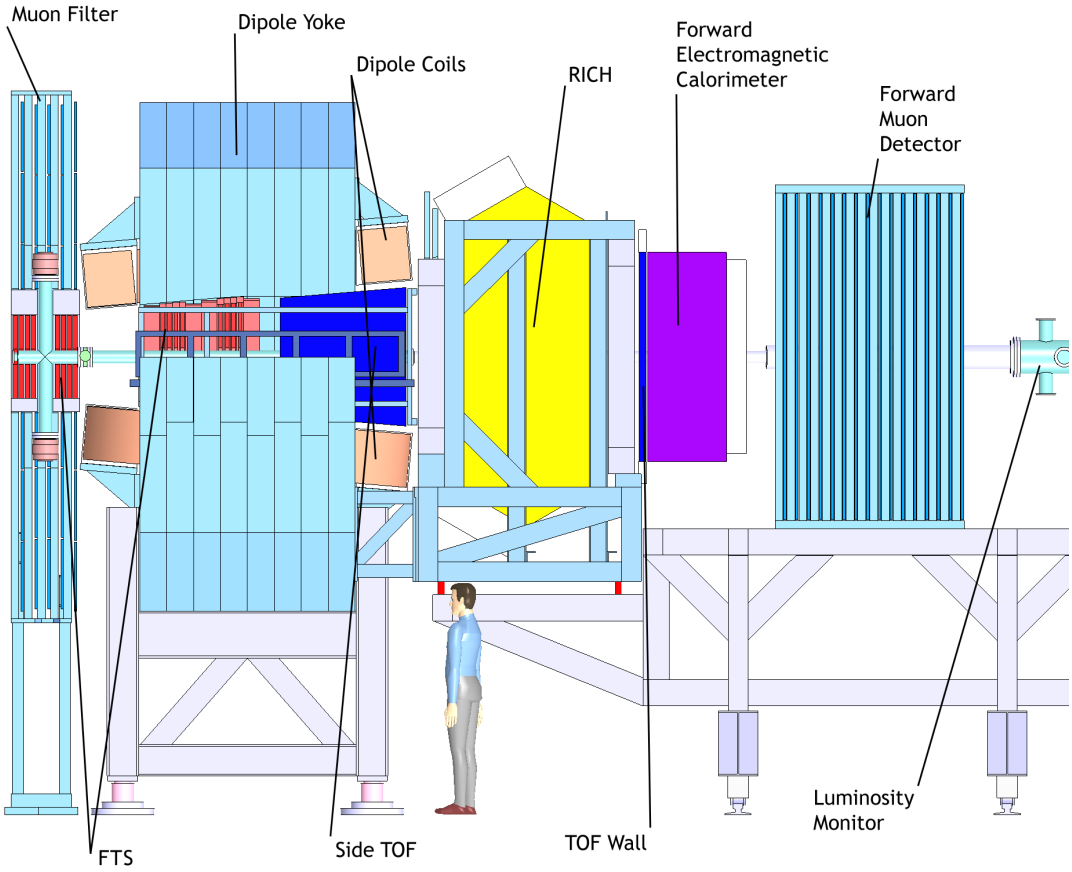

Figure 2.5: Side view of $\overline{\mathrm{P}}$ANDA forward Spectrometer (FS). The antiproton beam enters from the left.

3 Requirements

Section 3.1 describes the expected event rates for phase 1 physics Section 3.2 discusses the pileup situation Section 3.3 discusses the available capacity for on-line storage and the resulting requirements on event filtering Section 3.4 discusses the partitioning of DAQ and DAQ running modes

3.1 Event rates for Phase 1 Physics

3.2 Pile-up situation

3.3 On-line storage and requirements for event filtering

3.4 DAQ partioning and running modes

Bibliography

4 System Architecture

Section 4.1 describes the basic building blocks of the system (SODAnet, data concentrators, data transport, FPGA based compute nodes, CPU/GPU farm) Section 4.2 describes data formats, interfaces and data flow Section 4.3 describes the event filtering system and its partitioning into FPGA based and CPU/GPU based algorithms Section 4.4 discusses run control (RC), error handling and data quality monitoring (DQM)

4.1 Basic building blocks of the system

4.2 Data formats, interfaces and data flow

4.3 Event filtering and partitioning of algorithms

4.4 Run Control, error handling and data quality monitoring

Bibliography

5 Performance

Section 5.1 describes discrete event simulations demonstrating the performance of the data acquisition system

Section 5.2 describes measurements with prototype components of the data acquisition system

5.1 Simulations

5.1.1 Framework

5.1.2 Results

5.2 Measurements with prototype components

5.2.1 Setup

5.2.2 Results

Bibliography

6 Project managements and ressources

6.1 Responsibilities

6.2 Schedule and Milestones

6.3 Cost

Bibliography

7 Acknowledgements

We acknowledge financial support from ...

List of Figures

List of Tables